PAPER

Elucidating the role of surfactant structural parameters in Au nanoparticle morphology

Debashree Roy [a] and Liane M. Moreau *[ab]

The use of cationic quaternary ammonium halide as a surfactant is popular in aqueous seed-mediated growth methods of noble metal nanoparticles (NPs). Despite the effective shape control of NPs that can be achieved by modifying the surfactant chemistry, these structural parameters have been insufficiently probed. The number of cationic quaternary ammonium halide surfactants explored for the synthesis of Au NPs have been limited primarily to cetyltrimethylammonium bromide (CTAB) and cetyltrimethylammonium chloride (CTAC). In this study, we investigate the effect of structural parameters, including the headgroup, chain length, and counter-anion of the quaternary ammonium halides, on the resultant Au NPs formed using seed-mediated synthesis. By employing pentatwinned Au NPs as the starting seeds, we observe that (i) increasing the bulkiness of the surfactant headgroup results in the formation of Au NPs with fewer stellations and more shape polydispersity, (ii) surfactant chain length affects the dimension of Au NPs, and (iii) the counter-anion associated with the surfactant affects the Au NPs' final morphology. These structural parameters provide a practical handle to tune the shape, size, and polydispersity of the final Au NPs.

Introduction

Seed-mediated growth is a versatile synthetic procedure which has resulted in an extensive library of anisotropic Au nanoparticles (NPs) of differing shapes and sizes, bound by both low and high index facets.[1,2] The easy tunability and reproducibility have become the hallmark of seeded growth, since its inception to synthesize Au nanorods (NRs), one of the most extensively studied anisotropic metal systems.[3] The seed-mediated growth comprises of a two-step process wherein "seeds" synthesized in the first step are subjected to overgrowth in the second step.[4] The separation of heterogeneous nucleation from homogeneous nucleation offers a way to reduce the polydispersity of the NP systems, both in shape and size, the success of which is reflected in the high shape yield associated with the anisotropic Au NPs synthesized using this route.[5]

Much of the success of aqueous seed-mediated synthesis of noble metal NPs has been attributed to the surfactants known to modulate their morphology as a shape-directing agent whilst also acting as capping agents.[6–8] The significance of surfactants is not just limited to aqueous seed-mediated synthesis, but other colloidal syntheses of metal NPs as well.[7,9–11] Here the surfactant chemistry plays a crucial role both during synthesis, by directing anisotropic growth while preventing aggregation of the NPs,[12] and post-synthetically influencing the surface functionalization of the NPs, which is expected to have direct consequences in applications ranging from catalysis[13–18] to drug delivery.[19–21] Quaternary ammonium halide surfactants commonly used in these syntheses are understood to direct the anisotropic growth of the Au NPs by capping specific facets of the Au NPs and stabilizing them, thereby modulating the growth direction.[22] Additionally, the halides present in these surfactants are also known to modify the redox potential of the metal ion apart from providing facet-specific capping.[5,23–25] These cationic surfactants self-assemble into micelles, above their critical micelle concentration (CMC) – a concentration usually maintained for the synthesis of Au NPs via the aqueous seed-mediated route. The morphological arrangement adopted by cationic surfactants in water can range anywhere from spherical, to cylindrical, to bilayer due to the dependence on the surfactant structure under relevant solution conditions as is evident from numerous prior studies.[26–33] Increasing the surfactant concentration gradually leads to the transformation of spherical micelles into cylindrical micelles via coalescence, which eventually leads to the formation of bilayers.[34–36] This structural transition in micelles take place at higher surfactant concentration as there is an increase in the number density of the counterions due to the dissociation of the surfactants. This increases the ionic strength of the solution, thereby reducing the electrostatic repulsion based on increased water coordination. The direct outcome of this is the increase in the value of the geometrical parameter referred to as the critical packing parameter (CPP). This parameter regulates the surfactant behaviour in the solution where a larger CPP value is associated with lesser curvature of the micellar aggregates.[35,36]

*a*Department of Chemistry, Washington State University, Pullman, WA 99164, USA
*b*Department of Chemistry, University of Wyoming, Laramie, WY 82071, USA. E-mail: lmoreau1@uwyo.edu

Two widely accepted mechanisms of surfactant arrangement on Au NPs are the formation of micelles and closed bilayers.[22,37] These studies which are mostly focused on Au NRs,[38–41] have confirmed the formation of a cetyltrimethylammonium bromide (CTAB) bilayer with a thickness between 30 and 34 Å,[42] where the outer layer has been found to be in equilibrium with the free surfactants in solution.[43] Even within individual particles, the surfactant density has been found to vary, with higher density of surfactant at the sides and a significantly reduced surfactant density at the tips of the Au NRs.[44] On the other hand, formation of patchy or discrete globular micelles has been reported for cetyltrimethylammonium chloride[45] (CTAC) which corroborates well to the poor shape yield of Au NRs associated with CTAC. Additionally, the micellar packing around the Au NP surface has been observed to be altered in the presence of additives/co-surfactants affecting the product yield.[46–50] Based on these aforementioned observations, it can be inferred that small changes to the structural attributes of the surfactant can have larger implications on the micellar morphologies and their organization on the Au NP surface, affecting the final resulting Au NP morphology.

Previous studies have found a direct correlation between increasing surfactant chain length and increasing NP size for NPs synthesized both photochemically as well as under aqueous conditions.[51,52] Still other studies have observed significantly altered morphologies upon changing the alkyl chain length of quaternary ammonium halide based surfactants.[53,54] Different studies investigating the effect of surfactant headgroup concluded that the presence of a bulkier headgroup slowed the precursor reduction rate enabling better morphological control.[53,55–57] The role of the counterion in the quaternary ammonium halide based surfactants has been examined previously in Au NP syntheses resulting in entirely different morphologies despite changing the halide species.[23,58–61] The addition of co-surfactants provides even greater tunability in NP morphology. For example, modifying the chain length of a co-surfactant in a binary mixture of quaternary ammonium halide-based surfactants has been observed to affect the yield and dimension of Au NRs.[62–64] In the cases of both single and co-surfactant systems associated with quaternary ammonium halide-based surfactants commonly employed in the aqueous seed-mediated synthesis of noble metal NPs, their structural parameters associated with anisotropic growth have never been studied in detail before through a thorough systematic investigation.

The formation of two distinct morphologies (pentatwinned NRs and decahedra) in the presence of two surfactants CTAB and benzyldimethylhexadecylammonium chloride (BDAC) which differ in their respective counter anion and polar head groups shows that the pentatwinned seeds are more susceptible to structural parameter changes of the surfactant.[65,66] This makes the penta-twinned seeds ideal candidates to undertake an investigation to study the effect of structural parameters associated with quaternary ammonium halides. Additionally, the propensity of single crystalline seeds to result in Au NRs in the presence of bromide and Ag$^+$ also makes it difficult to study other structural parameters associated with these quaternary ammonium halides.[67–69]

In the present work, we investigate the dependence of the structural parameters associated with the quaternary ammonium halide surfactants on the resultant Au NP morphology at concentrations much higher than their CMC, mimicking concentration typically maintained for seed-mediated aqueous synthesis. The quaternary ammonium halide-based surfactants are a class of cationic surfactants whose structural parameters can be divided into three segments – the polar headgroup, the non-polar hydrocarbon chain acting as the tail, and the halide counter anion associated with the headgroup.[6] Because of solubility and stability issues, these cationic surfactants are mostly available in their chloride and bromide forms only. To examine the effect of the polar headgroup, we studied the $C_{16}TAC$ analogues, CTAC, cetylpyridinium chloride (CPC), and BDAC with different headgroups, while the length of the non-polar hydrocarbon chain and the chloride counterion were unchanged (Scheme 1). This allowed us to understand the steric effect associated with the headgroup in modifying the final NP. We found that increasing the bulkiness of the headgroup resulted in Au NPs with lesser branching and narrower arms and more shape polydispersity. To understand how changing the surfactant counterion would affect the growth of penta-twinned seeds, both $C_{16}TAX$ and $C_{16}PX$ (X = Cl/Br) surfactants were explored in the syntheses. The chloride-based surfactants resulted in stellated morphologies; however, no defined morphology could be assigned to the Au NPs generated from the corresponding bromide counterparts. The chain length of the surfactant not only determines the hydrophobicity of the surfactant but is also crucial for interchain packing of the surfactant bilayer on the Au surface.[70] Thus, when the penta-twinned seeds were subjected to growth in presence of surfactants (C_{16}-BDAC *vs.* C_{14}-BDAC) which varied only in the hydrocarbon chain length, the dimension of the Au NPs was affected more than the resultant morphology.

Carrying out a systematic variation of surfactant structural parameters on the final Au NP morphology allows us to interpret the precise chemical interactions that lead to the observed morphological changes. Our findings provide a more wholistic picture of the role of the quaternary ammonium surfactants in seed-mediated growth of Au NPs that can be implemented to other metal NP systems as well which make use of these
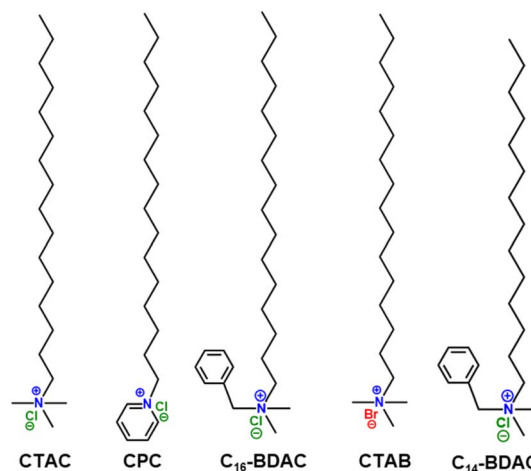
Scheme 1 A schematic representation of the chemical structure of the different surfactants used in the present study.

surfactants. Furthermore, we realize that binary surfactants, where either $C_{16}PX$ or $C_{16}TAX$ (X = Cl) is present in excess over other chloride or bromide-based surfactants, wield better control over shape than using a single surfactant and the resultant Au NPs displayed more defined stellations. Overall, the structural parameters of the surfactants obtained from small angle X-ray scattering (SAXS) were consistent with the observations from scanning electron microscopy (SEM) and nuclear magnetic resonance (NMR) data collected for Au NPs synthesized with these surfactants, allowing us to arrive at our conclusions as dictated in Scheme 2, namely (1) increasing the surfactant headgroup bulkiness leads to fewer stellations, (2) increasing the surfactant chain length increased the resulting particle size, and (3) changing the counter anion species affected the formation and sharpness of the NP stellation. Surprisingly, when the binary surfactants were employed under seedless conditions, only the bromide containing binary surfactant mixture resulted in the formation of stellated Au NPs while the chloride-only binary surfactant mixture continued to generate concave cube Au NPs.

Materials and methods

Chemicals

Silver(I) nitrate (>99.99%), gold(III) chloride trihydrate, tannic acid, cetyltrimethylammonium chloride, cetylpyridinium chloride, cetylpyridinium bromide, benzyldimethylhexadecylammonium chloride, benzyldimethyltetradecylammonium chloride, and sodium borohydride were purchased from Aldrich. Sodium hydroxide (ACS-grade) was bought from Macron and cetyltrimethylammonium bromide was purchased from Bioworld. Citric acid was purchased from J. T. Baker Inc. All chemicals were used as received without additional purification. All H_2O used to make solutions was UltraPure Type 1 Deionized Water (ChemWorld). All glassware was washed with aqua regia and dried under nitrogen prior to use. To prepare 5 mL of 200 mM surfactant solutions, respective amounts of the surfactants (CTAB, CPC, CPB, C_{16}-BDAC, C_{14}-BDAC) were weighed out and dissolved completely in ultrapure DI water to obtain a clear solution which was stored in a 100 mL glass reagent bottle. A 5 mL 200 mM CTAC solution was prepared using CTAC solution (25 wt% in H_2O) purchased from Sigma-Aldrich. All surfactant and tannic acid solutions used were prepared immediately prior to the syntheses, while gold and silver precursor solutions were prepared and stored in amber glass reagent bottles for approximately one week.

Synthesis of pentatwinned Au NPs used as seeds

The synthesis of Au pentatwinned NPs used in the present study was carried out by following a previously reported synthetic protocol.[66] Au pentatwinned NPs generated in high yield were subjected to overgrowth without further purification. Briefly, to an aqueous 50 mM CTAC solution, 10 mL 0.25 mM $HAuCl_4$ and 5 mM citric acid were added, followed by the addition of 0.25 mL of 25 mM freshly prepared $NaBH_4$ solution under vigorous stirring at room temperature which turned the solution from light yellow to brown. The round-bottom flask was closed after 2 minutes and the solution was heated at 80 °C for 90 minutes under gentle stirring.

To prevent explosion of the flask, a needle was inserted through a Teflon tape sealing to prevent positive pressure build-up. The colour of the solution changed from brown to red and the seed solution was removed from heat and stored in a glass vial at room temperature for months without disintegration.

Synthesis of stellated Au NPs using a single surfactant

To synthesize Au NPs, we developed a novel synthetic route. A growth solution was prepared by adding 702 μL UltraPure DI water, 1 mL, 200 mM CTAC (CPC, C_{16}-BDAC, C_{14}-BDAC, CTAB or CPB), 250 μL 4 mM $HAuCl_4$, 10 μL 4 mM $AgNO_3$, and 20 μL 100 mM NaOH. This was followed by the addition of 10 μL 100 mM tannic acid which resulted in a color change of the solution from yellow to pale tan. Following the color change, 8 μL of the pentatwinned seed solution was introduced to the growth solutions to initiate the reaction and left undisturbed overnight. The resultant Au NPs were centrifuged three times at 9900 × g RCF for 5 minutes where the supernatant was discarded while the pellet of the particles was redispersed in ultrapure DI water. After three rounds of centrifugation, the volume was reduced 10 times from the starting Au NP solution to maintain a final volume of 200 μL of purified Au NPs redispersed in ultrapure DI water. This was used for further characterization which was performed within days of the syntheses. The particles were confirmed to be stable for up to 3 months.

Synthesis of stellated Au NPs using a binary surfactant mixture

A novel synthetic protocol was devised which is outlined below. To synthesize Au NPs, a growth solution was prepared by adding 702 μL UltraPure DI water, 750 μL 200 mM CTAC or CPC and 250 μL 200 mM CTAB or C_{16}-BDAC or C_{14}-BDAC (to make the volume up to 1 mL), 250 μL 4 mM $HAuCl_4$, 10 μL 4 mM $AgNO_3$, and 20 μL 100 mM NaOH. This was followed by the addition of 10 μL 100 mM tannic acid which resulted in a color change of the solution from yellow to pale tan. Following the color change, 8 μL of the pentatwinned seed solution was introduced into the growth solutions to initiate the reaction and left undisturbed overnight. The resultant Au NPs were centrifuged thrice at 9900 × g RCF for 5 minutes for purification and to enable further characterization. For the seedless control condition, no seed solution was introduced into the growth solution.

Scanning electron microscopy (SEM)

All SEM images were collected using an FEI Apreo VolumeScope SEM. The samples for SEM imaging were prepared by dispersing the washed sample in DI water, so that the final volume was 200 μL. 10 μL of the respective sample dispersions were drop-cast on ultra-flat Si wafers and allowed to dry overnight in a desiccator. The size analysis on the Au NPs was carried out manually using ImageJ software on over 100 particles for each sample. The images were collected over 5 places on the Si wafer.

Small angle X-ray scattering (SAXS)

A Xenocs Xeuss 3.0 HR SAXS instrument was used to collect data using a Cu source. The identical concentration and volume of the

surfactant used in the synthesis were maintained to prepare the solution for measurement. UltraPure water (18.2 MΩ) was added so that the resultant concentration of the surfactants used for synthesis was maintained (100 mM). The surfactant solutions were then placed in 1.5 mm quartz capillaries for measurement with a slit size of 0.35 × 0.7 mm. The scattering intensity of Au NPs being much higher than that of the surfactants, all measurements were carried out only on the surfactant solution to extract useful data. Raw CCD images containing 2D scattering patterns were reduced to 1D q-space patterns in XSACT software. The sample-to-detector distance was 370 mm and was calibrated using the pattern of a silver behenate calibrant. 2D patterns were azimuthally averaged to extract the 1D patterns.

Nuclear magnetic resonance (NMR) spectroscopy

^{1}H NMR spectra were obtained using a Bruker Advance Neo 500 MHz spectrometer with a Bruker iProbe probe. The number of scans was set to 256, with a delay time of 1.0 s, and a line broadening of 0.30 Hz for the surfactants while the number of scans was increased to 1024 for the Au NPs while keeping all other parameters the same. Surfactant solutions were prepared in D_2O, maintaining a resultant concentration of 100 mM. Aqueous NP solutions were centrifuged (same centrifuge conditions used as for NP purification) and re-dispersed in UltraPure water three times prior to measurements to remove any unreacted species. The Au NPs were resuspended in pure D_2O after washing.

Results and discussion

The current study takes an extensive look at the structural parameter aspect of the quaternary ammonium halide-based surfactants which are commonly employed in aqueous seed-mediated synthesis of noble metals, especially Au NPs. A systematic approach is employed to understand individually how the steric, hydrophobic, and electrostatic effect associated with the head-group, hydrocarbon chain length, and counter-anion respectively affects the final NP morphology (Scheme 1). To provide a comprehensive understanding, both seed-mediated synthesis employing a pentatwinned starting seed as well as a seedless approach have been employed.

Bulky headgroups result in Au NPs with fewer stellations and more shape polydispersity

The effect of the surfactant sterics on NP morphology was investigated by employing three chloride-based surfactants with identical chain length but differing headgroup bulkiness, namely CTAC, CPC, and BDAC in an increasing order of bulkiness respectively. These cationic surfactants differing only in their headgroup were probed using SAXS to enable us to interpret the effect of the surfactant headgroup on the intermicellar and intramicellar interactions (Fig. 1d). Previous studies have shown the formation of micelles for such cationic surfactants, while vesicle formation was attributed to the presence of mixed cationic anionic surfactants.[29,71–73] Fig. 1d exhibits the scattering cross-section of the three chloride-based surfactants with identical chain lengths and counter anion at the same resultant
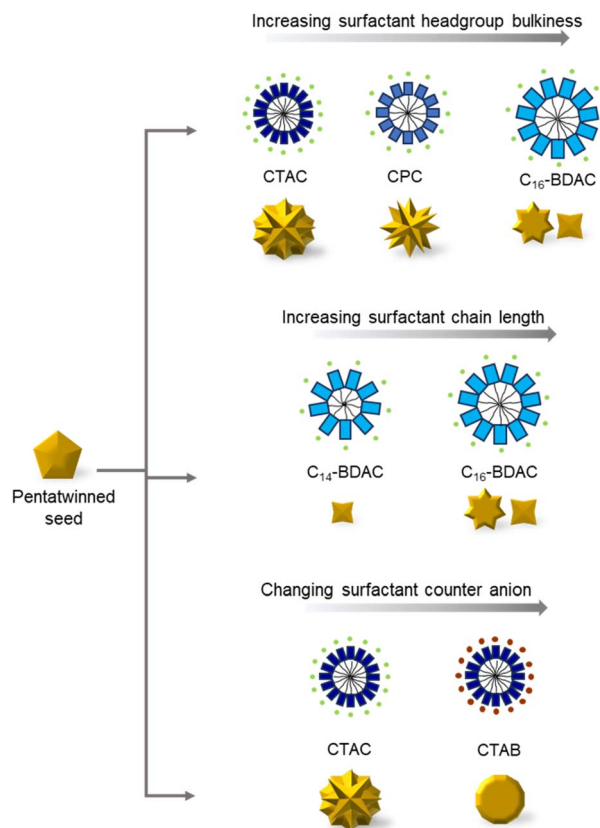

Scheme 2 Summary of the effect of variation of different surfactant structural parameters, headgroup, chain length, and counter-anion on the final Au NP morphology from a pentatwinned Au seed.

concentration (0.1 M). The scattering cross-sections for all three cationic surfactants are characterized by a peak and a shoulder which indicates the formation of a core–shell form factor that arises as the chloride counterion condenses inside the polar shell of the micelle. The inset in Fig. 1d is a representative image of the core–shell micellar structure adopted by the surfactant, with a hydrocarbon micellar core and a polar shell. The contrast difference between the micellar core and the solvent and that between the polar shell and the solvent vary according to the electron density of the atoms involved. This gives rise to a form factor peak which results in a double peak, typically associated with core–shell form factors in SAXS.[74] The intermicellar repulsion arising for the three cationic micelles give rise to strong structural factor contributions resulting in a correlation peak (q_{corr}). The mean intermicellar distance, d_{im}, thus can be derived from the q_{corr} peak as $d_{im} = 2\pi/q_{corr}$. The q_{corr} values obtained from the SAXS data were found to follow the order CTAC < CPC < BDAC (Table S1), leading to mean intermicellar distance values which follow a reverse order (CTAC > CPC > BDAC). Similar values reported previously for the said surfactants at a concentration of 0.1 M lend credibility to our findings.[70,74,75] Thus, the higher d_{im} values associated with CTAC indicate that it forms fewer micelles (indicated by low number density N_d) with more molecules per micelles (represented by higher aggregation number N_{agg}) than CPC which in turn forms fewer and larger micelles when compared to BDAC
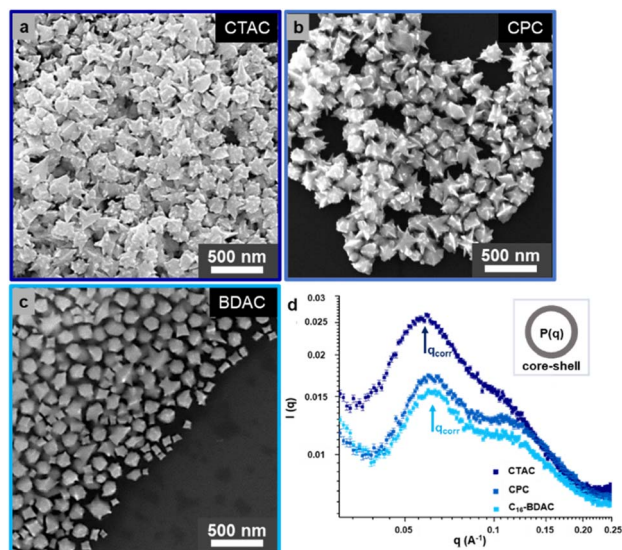
Fig. 1 (a–c) SEM images of Au NPs synthesized using surfactants with increasing headgroup bulkiness show the formation of Au NPs with fewer stellations and increased shape polydispersity. (d) SAXS patterns of surfactants having the same chain length and counter anion but different headgroups, CTAC, CPC, and BDAC, indicate changing peak positions and scattering intensity. Inset (d): Representative image of the core–shell micellar structure adopted by the surfactant.

as the same total number of molecules are present in the solution (0.1 M). Moreover, the low scattering cross-section observed for CPC and BDAC can be attributed to the electron resonance within the benzene headgroup. The second peak observed in the SAXS curve at higher q values arises from the scattering of the condensed chloride counter anions arranged around the micelles as the polar shell.[70,74,75]

The corresponding electron microscopy images (Fig. 1a–c) of Au NPs synthesized using these surfactants show that increasing the bulkiness of the headgroup not only resulted in fewer branches but also narrower arms. BDAC with the bulkiest headgroup among the three not only resulted in less branched Au NPs but also a sizable proportion of concave cube Au NPs. Additionally, a minor reduction in dimension of the Au NPs was observed with increase in the headgroup size. Since these surfactants form a bilayer on the Au NP surface with the polar headgroup binding to the metal surface, the bulkiness of the headgroup will dictate the packing density of the surfactants and hence the permeability of the metal atoms being reduced.[27] Thus, CTAC with the least bulky headgroup among the three will have the most closely packed surfactant layers on the Au surface while BDAC will have the most loosely packed surfactant bilayer as determined from our SAXS data. This will enable more diffusion of the Au atoms to the Au surface resulting in Au NPs with bigger core and fewer arms when BDAC was employed. Since diffusion will be restricted in the closely packed surfactant bilayer, deposition will dominate giving rise to wider arms for Au NPs synthesized using CTAC.

Surfactant chain length affects the dimension of Au NPs

The correlation of the surfactant chain length with the Au NP morphology was investigated by using chloride-based

surfactants with identical polar headgroups but different chain lengths (C_{16}-BDAC vs. C_{14}-BDAC). The SAXS data obtained for C_{16}-BDAC and C_{14}-BDAC show that they are strongly influenced by the surfactant chain length (Fig. S1a). The chain length and therefore the volume of the hydrophobic tail of the surfactants are known to determine the core radius of the micelle. A smaller core radius will arise from the C_{14}-BDAC in comparison to the C_{16}-BDAC.[26,76] Thus, the size of the micelle can be varied simply by changing the length of the hydrophobic tail of the surfactants as observed from the corresponding SAXS curves where the correlation peak q_{corr} for the shorter chain BDAC surfactant appears at higher q values indicating a decrease in the average intermicellar distance d_{im} for C_{14}-BDAC (Table S2).

To accommodate the extra hydrocarbon present in C_{16}-BDAC over C_{14}-BDAC in the micellar core, not only do we observe the formation of a larger micelle but also the formation of an ellipsoidal micelle instead of a spherical micelle. The width of the peak is correlated with the charge on the micelles.[30] We observed that with increase in the hydrocarbon chain length, there is an increase in the concentration of the counter anions bound to the micellar shell, which enables the screening of headgroup repulsion, bringing the headgroups closer and reducing the charge on the micelles. These observations resonate with previous findings where smaller micelles with more fractional charges on the shell were observed for shorter chain length cationic surfactants than their longer chain counterparts.[31,77]

Previous studies on Au nanorods (NRs) carried out by systematic variation of surfactant chain length (C_{10}–C_{16}) showed that increasing the hydrocarbon chain length resulted in the formation of longer NRs irrespective of whether a seed-mediated method or a photochemical method was employed.[51,52] On the other hand, a reverse correlation between the chain length of the ligand to the NP size was realized in hot injection methods commonly employed to synthesize semiconductor NPs.[78] In the present study, our observations are in line with those observed for seed-mediated Au NRs. C_{14}-BDAC gave rise to concave cube Au NPs with average length 44 ± 5 nm and average width 34 ± 5 nm, which is almost half when compared against the concave cube Au NPs generated using C_{16}-BDAC (average length 86 ± 14 nm and average width 61 ± 12 nm) (Fig. 2). The longer chain surfactant resulted in a mix of concave cube Au NPs and stellated Au NPs, while a better shape uniformity was achieved with the shorter chain surfactant. This observation can be rationalized by considering that increasing the surfactant chain length results in the formation of ellipsoidal micelles instead of spherical micelles, allowing greater diffusion of the reduced Au atoms at the micellar ends for the C_{16}-BDAC surfactant. This gives rise to larger Au NPs. The anisotropic micellar morphology was also responsible for the poor shape uniformity arising from C_{16}-BDAC. For the C_{14}-BDAC we observe an isotropic micelle due to its spherical shape. This results in smaller and more uniform concave cube Au NPs.

Surfactant counter-anion affects the morphology of the Au NPs

Comparing the influence of the surfactant counterion on SAXS patterns of CTAC and CTAB, we find that the effect on the
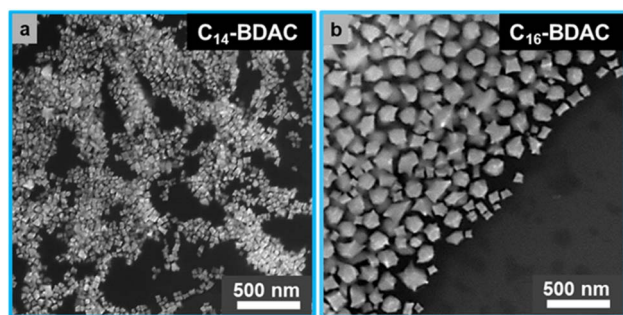
Fig. 2 (a and b) SEM images of Au NPs synthesized using surfactants with increasing hydrocarbon chain length show the formation of Au NPs with increasing dimension.

intermicellar interactions is more prominent than the effect of the headgroup chemical structure. Given that the surfactants have identical structural parameters except for the halide counter anion, we observe that the SAXS patterns are significantly different from one another as corroborated from literature reports.[32,70,74] The intermicellar distance of CTAB determined from q_{corr} was found to be longer than that of CTAC (Table S3). This is in line with previous reports which point towards the formation of fewer but larger micelles for CTAB than CTAC at the same concentration (0.1 M).[32,70,74] The increase in micellar size is also indicative of more ellipsoidal shaped CTAB micelles when compared to CTAC. This difference arises due to the condensation behaviour of the counter anion. The chloride counter anions generate stronger intermicellar repulsion that results in an enhanced structural factor for CTAC. The bromide counter anions on the other hand are bound more efficiently providing better electrostatic screening and hence weaker intermicellar repulsion. This determination is further compounded by the lower electronic density of chloride than bromide, as scattering varies as the square of the electron density of the atom, hence resulting in weaker scattering contrast. Taken together, these factors contribute to a higher scattering cross-section magnitude for CTAC micelles as is observed in Fig. S1b. The prominent shoulder in the SAXS curve associated with CTAB is indicative of a higher concentration of counter anions having higher contrast condensed within the polar shell, thereby enhancing the form factor contribution of the core–shell. Thus, it can be inferred that the presence of bromide ions forms a more compact monolayer around the CTA$^+$ micelle than the layer formed in the presence of chloride ions. This will have implications on atom deposition and diffusion as will be subsequently discussed.

The influence of surfactant counter-anion has been investigated previously in the context of seed-mediated synthesis of Au NPs where single crystalline NPs have been employed as starting seeds. We explore the effect of the halide counter-ion in the overgrowth of the pentatwinned Au seeds by employing two sets of C$_{16}$-based surfactants, C$_{16}$TAX and C$_{16}$PX (X = Cl/Br). In both cases we observe that the chloride-based surfactants result in stellated structures whereas their bromide counterparts are unable to give rise to any defined Au NP morphology (Fig. 3). As demonstrated in previous studies, changing the halide counter anion associated

with the surfactant changes the reduction potential of the metal precursor and hence the rate of Au$^+$ reduction.[5,24,25,58] Thus, in the presence of chloride-based surfactants, the Au-chloride complex exists which is easier to reduce than the Au-bromide complex formed in the presence of the bromide-based surfactants.[5,58] In addition to this, the solubilities of the Au-halide complexes also decrease with increasing size of the corresponding halide, changing the effective Au$^+$ concentration in solution and hence the availability of Au$^+$ for reduction.[5,58] This is further compounded by the adsorbate binding strength of the halide to the Au NP surface by modifying the amount of surface area available for catalyzing the reduction of Au$^+$ to Au^0.[5,58] With binding strength of Cl$^-$ < Br$^-$, the corresponding desorption of the halide from the NP surface becomes increasingly difficult, lowering the Au surface area to facilitate the reduction of Au$^+$.[5,58] These parameters will affect the reduction rate of the precursor and thus the NP growth kinetics. Therefore, in the presence of the chloride-based surfactant the rate of Au atom generation being faster than that in the presence of the bromide-based surfactant, the rate of atom deposition (R_{dep}) exceeds the rate of atom surface diffusion (R_{diff}).[79–81] Consequently, the atom deposition takes place at the intrinsic strains present in the pentatwinned Au seeds which are unstable and associated with high energy along with the unprotected corners, to minimize the overall energy associated with the growing NPs. Since $R_{dep} \gg R_{diff}$, the position of the newly deposited atoms remains unchanged, subsequently transforming the pentatwinned seed into a stellated Au NP. On the other hand, in the presence of the bromide-based surfactants, a slower generation of the Au atoms allows for the migration of the newly deposited atoms to the edges and side faces of the pentatwinned seeds as $R_{diff} \gg R_{dep}$. Previous studies on the surfactant organization on Au surfaces have shown that CTAC
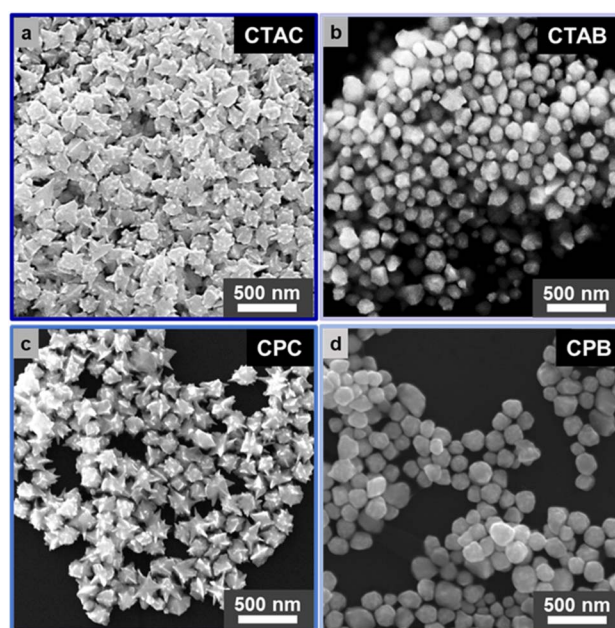

Fig. 3 (a–d) SEM images of Au NPs synthesized using different surfactants differing only in the counter-anion associated with the surfactant show that the final NP morphology is dramatically affected by changing the counter-anion.

gives rise to patchy or discrete micelle formation while CTAB generates a compact bilayer formation around the NP surface.[45] The presence of patchy CTAC micelles enables multiple channels for rapid Au deposition to take place on the pentatwinned seeds resulting in the stellated Au NPs we observe. On the other hand, the CTAB bilayers on Au NPs are just as compact as their free micelles in water, and the rate of Au atom generation is also significantly lowered than in the presence of CTAC. Taken together, the above reasons account for the absence of any stellation and defined morphology observed for the Au NPs.

The binary surfactant mixture leads to better morphological control of Au NPs

To further investigate the dependence of the Au NP morphology on the structural parameters of the surfactant, we performed the synthesis of Au NPs using a mixture of surfactants employed in the current study. This involved combining a chloride-based surfactant (CTAC or CPC) in excess with another surfactant having a different headgroup or chain length (C_{16}-BDAC or C_{14}-BDAC) or different counter anion (CTAB) while maintaining an overall constant surfactant concentration. Fig. 4 indicates that the stellations on the Au NPs are more defined in the presence of the binary surfactant mixture. We find that the presence of bromide in the surfactant mixture not only resulted in a defined number of arms, but also larger Au NPs. The same conclusion

holds for the CPC-dominated surfactant mixtures. The arrangement of mixed surfactants around the NP surface is still debatable with some attributing it to the formation of alternating stripes of similar surfactants on the NP surface,[82] while others have categorized it as Janus, patchy or random.[83,84] While a quantitative picture of the mixed surfactant arrangement around the NP surface is improbable for us, nuclear magnetic resonance (NMR), a non-destructive technique can give an idea about the surface landscape of the resultant Au NPs.[85] Although NMR for larger particles presents a complicated spectra with significant peak broadening[86,87] unlike what is observed in the present study, we cannot entirely rule out effects of ligand exchange in the solution or concentration-based effects. We used NMR to look at surfactants, obtaining reasonable data as have others, when one dimension of the particles is sufficiently small to allow for rotation of the ligand on the NP surface (in this case, the stellated tips, which are less than 25 nm in size). The ^{1}H NMR measurements carried out on the Au NPs exhibit peaks characteristic to both the surfactants used in the synthesis, thereby confirming that the usage of binary surfactants acts synergistically to improve the shape of the resultant Au NPs (Fig. S2–S7).[27,50,88–91] Additionally, the upfield shift of the proton peaks situated in the vicinity of the nitrogen head group indicates the interaction of the surfactant molecules with the Au NP surface through their headgroups. The SAXS data on the other hand collected for the mixed micelles exhibit the
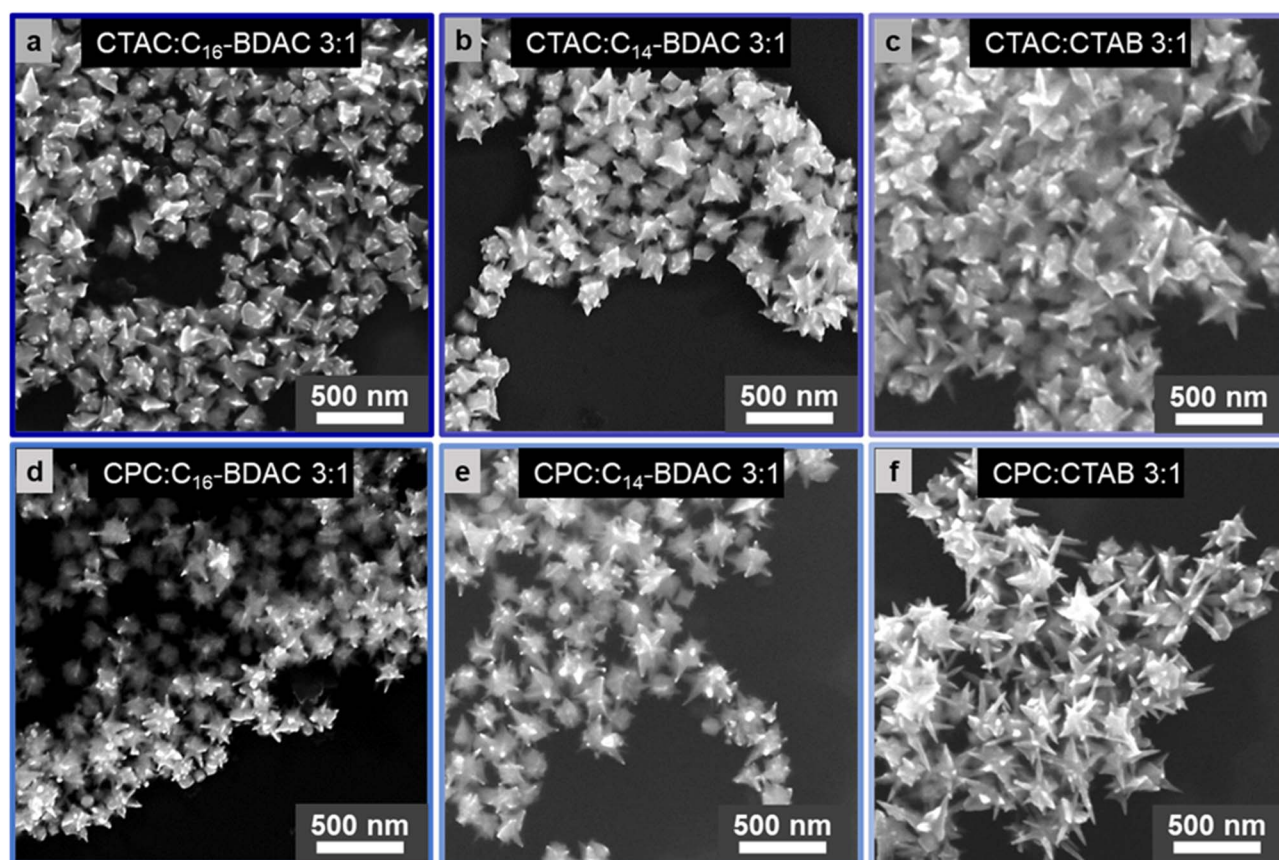

Fig. 4   SEM images of stellated Au NPs synthesized using (a–c) CTAC-based binary surfactant mixture and (d–f) CPC-based binary surfactants showing a better control over morphology.

correlation peaks which do not conform to the q_{corr} values of the individual surfactants (Fig. S8). As can be expected, the peak positions are similar to the dominating surfactant present in the solution (Tables S4 and S5). Unfortunately, other than endorsing the fact that the binary surfactants give rise to a mixed micelle instead of individual micelles, the SAXS data are unable to provide more information on their arrangement.[28] Our SAXS data, while suggesting that the binary surfactant mixtures are homogeneously bound, cannot rule out entirely the possibility that there may be local clustering.[82] We can only determine the intermicellar and intramicellar distances from the SAXS data, neither of which provides quantitative evidence for the mixed surfactant arrangement in these micelles. The presence of an additive/co-surfactant has been confirmed previously to modify the micellar arrangement around Au NPs.[6,46–50] We postulate that this modification can account for why more defined stellations are observed in the presence of the binary surfactants, especially when CTAB is present. When CTAB is present in the binary surfactant mixture, its concentration is not sufficient to enforce a compact bilayer around the Au NP surface nor is the Au NP surface surrounded by the patchy micellar globules of the chloride-based surfactant only. The presence of the binary surfactant changes the individual micellar arrangement around the Au NPs. This results in narrower channels for Au atom deposition giving rise to Au NPs with the most well-defined stellations (Fig. 4c and f). Surprisingly, when the same reactions were carried out in the absence of any seeds, it was found that only in the presence of bromide-based surfactants did the formation of the stellated Au NPs take place (Fig. S9). The chloride-based binary surfactant mixtures irrespective of the surfactant headgroup or chain length consistently resulted in the formation of the concave cube Au NPs. In our earlier work we have shown that decahedral Au NPs with five-fold twinning and bound by {111} planes gave rise to stellated NPs in the presence of a binary surfactant containing bromide, while giving rise to concave cubes in the presence of a chloride-based surfactant.[92] Additionally, in the seminal work by Mirkin and co-workers, Au concave cube NPs were generated when chloride-based surfactants were used both for the seed synthesis as well as the overgrowth.[93] Thus, it is not entirely surprising that concave cube Au NPs are formed in the chloride-based binary surfactant mixture. We postulate that when bromide is present in the surfactant mixture, the initial seeds formed are bound primarily by {100} planes and $R_{diff} < R_{dep}$ results in the deposition of the newly generated atoms at the corners resulting in stellated Au NPs that are observed.

Conclusions

In this work we have meticulously examined the structural parameters, headgroup, hydrocarbon chain length, and counter-anion, associated with quaternary ammonium halide-based surfactants commonly employed in the aqueous seed-mediated growth method of Au NPs. This was accomplished using SEM and NMR in conjunction with SAXS techniques which together provide thorough structural probes. Subjecting the pentatwinned seeds to overgrowth in the presence of surfactants whose parameters were systematically varied allowed us to observe the dominance of each individual parameter on the resultant Au NPs. We found that a less bulky headgroup allows for a closer packing of the surfactant bilayers enabling a tighter control over the shape yield, while the hydrocarbon chain length regulates the size of the resultant Au NPs. On the other hand, the counter-anion associated with the surfactant controls the shape of the final Au NPs. To the best of our knowledge this is the first instance of such a detailed investigation being undertaken on the structural parameters of the quaternary ammonium cationic surfactants in seed-mediated synthesis. We further realize that rationally tailored binary surfactant mixtures enable better morphological control over the resultant Au NPs, both with and without the presence of seeds. We anticipate that these findings will not only advance the synthetic methodology pertaining to Au NPs but also open up the understanding for other systems which make use of such surfactants.

Author contributions

The project was conceptualized by D. Roy, who also synthesized all particles and performed microscopy, NMR, and SAXS measurements. The manuscript was written by D. Roy and L. M. Moreau. All authors have given approval to the final version of the manuscript.

Conflicts of interest

There are no conflicts to declare.

Data availability

Data are included in the main text and supplementary information (SI). We have provided detailed protocols on how the data were collected. Our synthetic protocols are highly reproducible and all information pertaining to how to synthesize and purify the nanoparticles are included in the Methods section of the manuscript. If anyone would like to request the raw data collected from the instrumentation, we will share this upon request. We also encourage readers to reach out if they have trouble reproducing our results. Supplementary information: additional SEM images along with NMR and SAXS data supporting this manuscript have been included. See DOI: https://doi.org/10.1039/d5na00754b.

Abbreviations

NPs	Nanoparticles
NR	Nanorod
CTAB	Cetyltrimethylammonium bromide
CTAC	Cetyltrimethylammonium chloride
CPC	Cetylpyridinium chloride
BDAC	Benzyldimethylhexadecylammonium chloride
C_{14}-BDAC	Benzyldimethyltetradecylammonium chloride
CMC	Critical micellar concentration
SEM	Scanning electron microscopy
SAXS	Small angle X-ray scattering
NMR	Nuclear magnetic resonance

Acknowledgements

References

1 N. D. Burrows, A. M. Vartanian, N. S. Abadeer, E. M. Grzincic, L. M. Jacob, W. Lin, J. Li, J. M. Dennison, J. G. Hinman and C. J. Murphy, *J. Phys. Chem. Lett.*, 2016, **7**, 632–641.

2 Y. Xia, K. D. Gilroy, H. C. Peng and X. Xia, *Angew. Chem., Int. Ed.*, 2017, **56**, 60–95.

3 B. Nikoobakht and M. A. El-Sayed, *Chem. Mater.*, 2003, **15**, 1957–1962.

4 Y. Xia, Y. Xiong, B. Lim and S. E. Skrabalak, *Angew. Chem., Int. Ed.*, 2009, **48**, 60–103.

5 M. L. Personick and C. A. Mirkin, *J. Am. Chem. Soc.*, 2013, **135**, 18238–18247.

6 M. S. Bakshi, *Cryst. Growth Des.*, 2016, **16**, 1104–1133.

7 T. Song, F. Gao, S. Guo, Y. Zhang, S. Li, H. You and Y. Du, *Nanoscale*, 2021, **13**, 3895–3910.

8 J. Mosquera, D. Wang, S. Bals and L. M. Liz-Marzán, *Acc. Chem. Res.*, 2023, **56**, 1204–1212.

9 J. Xiao and L. Qi, *Nanoscale*, 2011, **3**, 1383–1396.

10 R. Xiao, J. Jia, R. Wang, Y. Feng and H. Chen, *Acc. Chem. Res.*, 2023, **56**, 1539–1552.

11 T. H. Yang, Y. Shi, A. Janssen and Y. Xia, *Angew. Chem., Int. Ed.*, 2020, **59**, 15378–15401.

12 R. M. Crooks, M. Zhao, L. Sun, V. Chechik and L. K. Yeung, *Acc. Chem. Res.*, 2001, **34**, 181–190.

13 Y. Shi, Z. Lyu, Z. Cao, M. Xie and Y. Xia, *Angew. Chem., Int. Ed.*, 2020, **59**, 19129–19135.

14 G. Collins, F. Davitt, C. O'Dwyer and J. D. Holmes, *ACS Appl. Nano Mater.*, 2018, **1**, 7129–7138.

15 H. Pu, H. Dai, T. Zhang, K. Dong, Y. Wang and Y. Deng, *Curr. Opin. Electrochem.*, 2022, **32**, 100927.

16 L. Wei, H. Li, J. Chen, Z. Yuan, Q. Huang, X. Liao, G. Henkelman and Y. Chen, *ACS Catal.*, 2019, **10**, 1444–1453.

17 X. Kong, J. Zhu, Z. Xu and Z. Geng, *Angew. Chem., Int. Ed.*, 2025, **64**, e202417562.

18 J. Newton, J. Preece, N. Rees and S. Horswell, *Phys. Chem. Chem. Phys.*, 2014, **16**, 11435–11446.

19 L. Wang, X. Jiang, Y. Ji, R. Bai, Y. Zhao, X. Wu and C. Chen, *Nanoscale*, 2013, **5**, 8384–8391.

20 M. Bhamidipati and L. Fabris, *Bioconjugate Chem.*, 2017, **28**, 449–460.

21 T.-L. Hwang, C. T. Sung, I. A. Aljuffali, Y.-T. Chang and J.-Y. Fang, *Colloids Surf., B*, 2014, **114**, 334–341.

22 S. K. Meena and M. Sulpizi, *Langmuir*, 2013, **29**, 14954–14961.

23 J. S. DuChene, W. Niu, J. M. Abendroth, Q. Sun, W. Zhao, F. Huo and W. D. Wei, *Chem. Mater.*, 2013, **25**, 1392–1399.

24 S. E. Lohse, N. D. Burrows, L. Scarabelli, L. M. Liz-Marzán and C. J. Murphy, *Chem. Mater.*, 2014, **26**, 34–43.

25 S. K. Meena, S. Celiksoy, P. Schäfer, A. Henkel, C. Sönnichsen and M. Sulpizi, *Phys. Chem. Chem. Phys.*, 2016, **18**, 13246–13254.

26 C. Tanford, *J. Phys. Chem.*, 1972, **76**, 3020–3024.

27 J. N. Israelachvili, D. J. Mitchell and B. W. Ninham, *J. Chem. Soc., Faraday Trans. 2*, 1976, **72**, 1525–1568.

28 H. Pilsl, H. Hoffmann, S. Hofmann, J. Kalus, A. Kencono, P. Lindner and W. Ulbricht, *J. Phys. Chem.*, 1993, **97**, 2745–2754.

29 R. Salkar, D. Mukesh, S. Samant and C. Manohar, *Langmuir*, 1998, **14**, 3778–3782.

30 V. Aswal and P. Goyal, *Phys. Rev. E:Stat. Phys., Plasmas, Fluids, Relat. Interdiscip. Top.*, 2000, **61**, 2947.

31 V. Aswal, P. Goyal, S. De, S. Bhattacharya, H. Amenitsch and S. Bernstorff, *Chem. Phys. Lett.*, 2000, **329**, 336–340.

32 V. Aswal, P. Goyal, H. Amenitsch and S. Bernstorff, *Pramana*, 2004, **63**, 333–338.

33 R. Nagarajan, *Langmuir*, 2002, **18**, 31–38.

34 P. Llombart, M. A. Palafox, L. G. MacDowell and E. G. Noya, *Colloids Surf., A*, 2019, **580**, 123730.

35 P. A. Hassan and S. L. Gawali, *Langmuir*, 2018, **35**, 9635–9646.

36 N. K. Raman, M. T. Anderson and C. J. Brinker, *Chem. Mater.*, 1996, **8**, 1682–1701.

37 B. Nikoobakht and M. A. El-Sayed, *Langmuir*, 2001, **17**, 6368–6374.

38 S. Seibt, H. Zhang, S. Mudie, S. Förster and P. Mulvaney, *J. Phys. Chem. C*, 2021, **125**, 19947–19960.

39 M. J. Hore, X. Ye, J. Ford, Y. Gao, J. Fei, Q. Wu, S. J. Rowan, R. J. Composto, C. B. Murray and B. Hammouda, *Nano Lett.*, 2015, **15**, 5730–5738.

40 B. T. Diroll, K. M. Weigandt, D. Jishkariani, M. Cargnello, R. J. Murphy, L. A. Hough, C. B. Murray and B. Donnio, *Nano Lett.*, 2015, **15**, 8008–8012.

41 S. Lee, L. J. Anderson, C. M. Payne and J. H. Hafner, *Langmuir*, 2011, **27**, 14748–14756.

42 S. Gomez-Grana, F. Hubert, F. Testard, A. Guerrero-Martínez, I. Grillo, L. M. Liz-Marzán and O. Spalla, *Langmuir*, 2012, **28**, 1453–1459.

43 F. Barbero, O. H. Moriones, N. G. Bastús and V. Puntes, *Bioconjugate Chem.*, 2019, **30**, 2917–2930.

44 B. E. Janicek, J. G. Hinman, J. J. Hinman, S. H. Bae, M. Wu, J. Turner, H.-H. Chang, E. Park, R. Lawless and K. S. Suslick, *Nano Lett.*, 2019, **19**, 6308–6314.

45 T. Zech, T. Schmutzler, D. M. Noll, M.-S. Appavou and T. Unruh, *Langmuir*, 2022, **38**, 2227–2237.

46 M. Bakshi and I. Kaur, *Colloid Polym. Sci.*, 2003, **281**, 10–18.

47 M. S. Bakshi and I. Kaur, *Colloid Polym. Sci.*, 2003, **281**, 935–944.

48 M. S. Bakshi, I. Kaur, R. Sood, J. Singh, K. Singh, S. Sachar, K. J. Singh and G. Kaur, *J. Colloid Interface Sci.*, 2004, **271**, 227–231.

49 J. Pérez-Juste, L. M. Liz-Marzán, S. Carnie, D. Y. Chan and P. Mulvaney, *Adv. Funct. Mater.*, 2004, **14**, 571–579.

50 X. Ye, L. Jin, H. Caglayan, J. Chen, G. Xing, C. Zheng, V. Doan-Nguyen, Y. Kang, N. Engheta and C. R. Kagan, *ACS Nano*, 2012, **6**, 2804–2817.

51 A. Kameo, A. Suzuki, K. Torigoe and K. Esumi, *J. Colloid Interface Sci.*, 2001, **241**, 289–292.

52 J. Gao, C. M. Bender and C. J. Murphy, *Langmuir*, 2003, **19**, 9065–9070.

53 D. Huang, Y. Qi, X. Bai, L. Shi, H. Jia, D. Zhang and L. Zheng, *ACS Appl. Mater. Interfaces*, 2012, **4**, 4665–4671.

54 M. Tsuji, K. Matsumoto, T. Tsuji and H. Kawazumi, *Mater. Lett.*, 2005, **59**, 3856–3860.

55 X. Kou, S. Zhang, C.-K. Tsung, M. H. Yeung, Q. Shi, G. D. Stucky, L. Sun, J. Wang and C. Yan, *J. Phys. Chem. B*, 2006, **110**, 16377–16383.

56 X. Kou, S. Zhang, C. K. Tsung, Z. Yang, M. H. Yeung, G. D. Stucky, L. Sun, J. Wang and C. Yan, *Chem.–Eur. J.*, 2007, **13**, 2929–2936.

57 Y. Liu, D. Liu, T. Li and Y. Liang, *ACS Appl. Nano Mater.*, 2023, **6**, 21312–21321.

58 M. R. Langille, M. L. Personick, J. Zhang and C. A. Mirkin, *J. Am. Chem. Soc.*, 2012, **134**, 14542–14554.

59 H. Kawasaki, K. Nishimura and R. Arakawa, *J. Phys. Chem. C*, 2007, **111**, 2683–2690.

60 Y. Hu, L. Wang, A. Song and J. Hao, *Langmuir*, 2018, **34**, 6138–6146.

61 M. Grzelczak, A. Sánchez-Iglesias, B. Rodríguez-González, R. Alvarez-Puebla, J. Pérez-Juste and L. M. Liz-Marzán, *Adv. Funct. Mater.*, 2008, **18**, 3780–3786.

62 M. Spirin, S. Brichkin, E. Yushkov and V. Razumov, *High Energy Chem.*, 2020, **54**, 308–315.

63 M. Spirin, S. Brichkin, A. Lizunova and V. J. C. J. Razumov, *Colloid J.*, 2022, **84**, 100–108.

64 O. Dement'eva, V. Matsur, A. Zaikin, N. Salavatov, M. Staltsov and V. J. C. J. Rudoy, *Colloid J.*, 2022, **84**, 689–695.

65 H.-L. Wu, C.-H. Chen and M. H. Huang, *Chem. Mater.*, 2009, **21**, 110–114.

66 A. Sánchez-Iglesias, N. Winckelmans, T. Altantzis, S. Bals, M. Grzelczak and L. M. Liz-Marzán, *J. Am. Chem. Soc.*, 2017, **139**, 107–110.

67 T. Sau and C. J. Murphy, *Philos. Mag.*, 2007, **87**, 2143–2158.

68 Y. Niidome, Y. Nakamura, K. Honda, Y. Akiyama, K. Nishioka, H. Kawasaki and N. Nakashima, *Chem. Commun.*, 2009, 1754–1756.

69 N. Almora-Barrios, G. Novell-Leruth, P. Whiting, L. M. Liz-Marzan and N. Lopez, *Nano Lett.*, 2014, **14**, 871–875.

70 V. Lutz-Bueno, R. Pasquino, M. Liebi, J. Kohlbrecher and P. Fischer, *Langmuir*, 2016, **32**, 4239–4250.

71 E. W. Kaler, K. L. Herrington, A. K. Murthy and J. A. Zasadzinski, *J. Phys. Chem.*, 1992, **96**, 6698–6707.

72 C.-Y. Leung, L. C. Palmer, B. F. Qiao, S. Kewalramani, R. Sknepnek, C. J. Newcomb, M. A. Greenfield, G. Vernizzi, S. I. Stupp and M. J. Bedzyk, *ACS Nano*, 2012, **6**, 10901–10909.

73 G. Changrui, L. Honghao, L. Yue, K. Sumit and O. de la Cruz Monica, *J. Phys. Chem. B*, 2017, **121**(7), 1623–1628.

74 V. Lutz-Bueno, M. Liebi, J. Kohlbrecher and P. Fischer, *Langmuir*, 2017, **33**, 2617–2627.

75 Y. Fan and Y. Wang, *Curr. Opin. Colloid Interface Sci.*, 2019, **42**, 1–16.

76 V. Aswal and P. Goyal, *Chem. Phys. Lett.*, 2002, **364**, 44–50.

77 S. Berr, *J. Phys. Chem.*, 1987, **91**, 4760–4765.

78 A. Sofie, S. Michael, J. Youngjin, C. Stefaan, L. Efrat and H. Zeger, *J. Am. Chem. Soc.*, 2015, **137**, 2495–2505.

79 Z. Lou, B. Huang, X. Qin, X. Zhang, H. Cheng, Y. Liu, S. Wang, J. Wang and Y. Dai, *Chem. Commun.*, 2012, **48**, 3488–3490.

80 H. Zhang, M. Jin and Y. Xia, *Angew. Chem., Int. Ed.*, 2012, **51**, 7656–7673.

81 A. Ruditskiy, H.-C. Peng and Y. Xia, *Annu. Rev. Chem. Biomol. Eng.*, 2016, **7**, 327–348.

82 C. Singh, Y. Hu, B. P. Khanal, E. R. Zubarev, F. Stellacci and S. C. Glotzer, *Nanoscale*, 2011, **3**, 3244–3250.

83 Z. Luo, D. Marson, Q. K. Ong, A. Loiudice, J. Kohlbrecher, A. Radulescu, A. Krause-Heuer, T. Darwish, S. Balog and R. Buonsanti, *Nat. Commun.*, 2018, **9**, 1343.

84 D. Roy, Y. Xu, R. Rajendra, L. Wu, P. Bai and N. Ballav, *J. Phys. Chem. Lett.*, 2020, **11**, 3211–3217.

85 K. M. Greskovich, K. M. Powderly, M. M. Kincanon, N. B. Forney, C. A. Jalomo, A. Wo and C. J. Murphy, *Acc. Chem. Res.*, 2023, **56**, 1553–1564.

86 M. Wu, A. M. Vartanian, G. Chong, A. K. Pandiakumar, R. J. Hamers, R. Hernandez and C. J. Murphy, *J. Am. Chem. Soc.*, 2019, **141**, 4316–4327.

87 K. M. Hatzis, X. Wei, M. Kincanon, A. Wo, J. Gandrapu, O. Zeiri, R. Hernandez and C. J. Murphy, *Chem. Mater.*, 2025, **37**(13), 4881–4893.

88 J. Ulmius, B. Lindman, G. Lindblom and T. Drakenberg, *J. Colloid Interface Sci.*, 1978, **65**, 88–97.

89 A. B. Mandal, L. Wang, K. Brown and R. E. Verrall, *J. Colloid Interface Sci.*, 1993, **161**, 292–298.

90 L. Okano, O. E. Seoud and T. Halstead, *Colloid Polym. Sci.*, 1997, **275**, 138–145.

91 K. Xu, H.-q. Ren, G.-m. Zeng, L.-l. Ding and J.-h. Huang, *Colloids Surf., A*, 2010, **356**, 150–155.

92 D. Roy, H. C. Larson, B. M. Cossairt and L. M. Moreau, *Nanoscale Adv.*, 2025, **7**, 4412–4418.

93 J. Zhang, M. R. Langille, M. L. Personick, K. Zhang, S. Li and C. A. Mirkin, *J. Am. Chem. Soc.*, 2010, **132**, 14012–14014.